Catalysis Letters (2021) 151:2816–2832
https://doi.org/10.1007/s10562-020-03519-y

Role of CO_2 During Oxidative Dehydrogenation of Propane Over Bulk and Activated-Carbon Supported Cerium and Vanadium Based Catalysts

Petar Djinović[1,5] · Janez Zavašnik[2,3] · Janvit Teržan[1] · Ivan Jerman[4]

Received: 21 August 2020 / Accepted: 24 December 2020 / Published online: 22 January 2021

Abstract

CeO_2, V_2O_5 and $CeVO_4$ were synthesised as bulk oxides, or deposited over activated carbon, characterized by XRD, HRTEM, CO_2-TPO, C_3H_8-TPR, DRIFTS and Raman techniques and tested in propane oxidative dehydrogenation using CO_2. Complete oxidation of propane to CO and CO_2 is favoured by lattice oxygen of CeO_2. The temperature programmed experiments show the ~ 4 nm AC supported CeO_2 crystallites become more susceptible to reduction by propane, but less prone to re-oxidation with CO_2 compared to bulk CeO_2. Catalytic activity of $CeVO_4$/AC catalysts requires a 1–2 nm amorphous $CeVO_4$ layer. During reaction, the amorphous $CeVO_4$ layer crystallises and several atomic layers of carbon cover the $CeVO_4$ surface, resulting in deactivation. During reaction, V_2O_5 is irreversibly reduced to V_2O_3. The lattice oxygen in bulk V_2O_5 favours catalytic activity and propene selectivity. Bulk V_2O_3 promotes only propane cracking with no propene selectivity. In VO_x/AC materials, vanadium carbide is the catalytically active phase. Propane dehydrogenation over VC proceeds via chemisorbed oxygen species originating from the dissociated CO_2.

Graphic Abstract

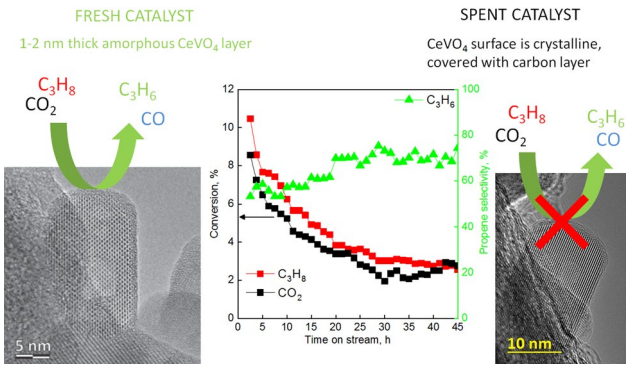

Keywords Propene · Oxidative dehydrogenation · CO_2 · Lattice oxygen · Reaction mechanism

Supplementary Information The online version contains supplementary material available at https://doi.org/10.1007/s10562-020-03519-y.

✉ Petar Djinović
petar.djinovic@ki.si

1 Department of Inorganic Chemistry and Technology, National Institute of Chemistry, Hajdrihova 19, 1000 Ljubljana, Slovenia

2 Jožef Stefan Institute, Jamova cesta 39, 1000 Ljubljana, Slovenia

3 Max-Planck-Institut Für Eisenforschung GmbH, Max-Planck-Straße 1, 40237 Düsseldorf, Germany

4 Department of Materials Chemistry, National Institute of Chemistry, Hajdrihova 19, 1000 Ljubljana, Slovenia

5 University of Nova Gorica, Vipavska 13, 5000 Nova Gorica, Slovenia

1 Introduction

Propene is an important commodity chemical in the petrochemical industry and is used for the synthesis of polypropylene, propylene oxide, acrylonitrile, cumene, butyraldehyde, acrylic acid, etc. It is currently produced in the amount of ~ 100 Mt/year, mainly by naphtha steam cracking and FCC (fluidised catalytic cracking) technologies. In recent years, a growing gap between the demand and supply of propene is becoming apparent, which calls for the implementation of additional propene production pathways [1]. Catalytic oxidative dehydrogenation of propane using O_2 or CO_2 emerge as possible solutions. The propane-O_2 ODH reaction is thoroughly researched and supported VO_x catalysts have been the focus of many experimental [2, 3] and theoretical studies [4]. The support strongly influences the performance of these catalysts and precise active site architecture is required to promote propane dehydrogenation instead of total combustion to CO_x [1]. Also, propane conversion and propene selectivity are strongly inversely connected due to facile activation of sp^2 hybridised C=C bond in propene, which promotes its further oxidation.

The propane-CO_2 ODH reaction (reaction 1) has some benefits, as well as drawbacks. It reduces CO_2 to CO and could be implemented for CO_2 valorisation and reduction of anthropogenic CO_2 emissions.

$$C_3H_8 + CO_2 \leftrightarrow C_3H_6 + CO + H_2O \qquad \Delta H_{298K} = 167\ \text{kJ/mol} \tag{1}$$

The reaction is endothermic, thermodynamically restricted, and favours carbon formation in a broad range of reaction conditions [5]. Thermodynamic analysis has shown that surplus CO_2 in the feed has the potential to alleviate the restricted equilibrium propane conversion and also lowers the tendency for carbon accumulation [6].

Propene weight time yield (gC_3H_6/g_{cat} h) is about two orders of magnitude lower with propane-CO_2 ODH compared to propane-O_2 ODH, which calls for the development of more active catalysts [7, 8]. Catalyst optimisation should start with understanding the active sites (requirements for propane and CO_2 activation), and continue by steering the catalyst synthesis towards their highest abundance.

Significantly higher propene selectivity (85 vs 20%) at 50% propane conversion demonstrates CO_2 as a superior oxidant in the propane ODH reaction [7, 9]. The high selectivity to the desired alkene originates from a selective formation of nucleophilic monoatomic O^{2-} ions when CO_2 dissociates on the catalyst's surface. Contrary, dissociation of O_2 leads to the formation of short-lived electrophilic oxygen species (O_2^- and O^-) before they are transformed to O^{2-}. These electrophilic oxygen species favour deep alkane/alkene oxidation [10, 11].

Several metal oxides (bulk and supported Ga_2O_3, Cr_2O_3, and Fe_2O_3) were tested by Michorczyk and Ogonowski [12] in the propane-CO_2 ODH reaction. Ga_2O_3 was identified as the most effective, with propene yield equal to 30% at 600 °C.

Zou et al. [13] investigated the effect of chromium loading in CrO_x/SiO_2 catalysts and established the following decreasing order of propane conversion and propene selectivity: 2.5 wt% CrO_x/SiO_2 > 5 wt% CrO_x/SiO_2 > 10 wt% CrO_x/SiO_2. UV–Vis spectroscopic analysis indicated that ODH activity correlates with highly dispersed chromates, such as Cr^{6+} ions in the form of mono, di and polychromates. With increasing chromium loading above 3 wt%, the presence of bulk Cr_2O_3 was identified. Deactivation of the catalyst with time on stream was observed and related to coke accumulation and changes in chromate speciation from oligomeric to bulk crystalline Cr_2O_3.

Martinez Huerta et al. [14] studied catalysts containing 2 and 5 wt. % vanadium dispersed over CeO_2 for ethane-O_2 ODH reaction. The *operando* Raman-GC analysis showed stepwise dispersion of V_2O_5 into surface VO_x, before the formation of the amorphous $CeVO_4$ phase. In the $CeVO_4$ phase, vanadium maintains its 5 + oxidation state and redox activity is related only to $Ce^{4+} \leftrightarrow Ce^{3+}$. The initially formed amorphous $CeVO_4$ converts into a well crystalline $CeVO_4$ phase as the reaction temperature increases. These authors also suggest that the V–O–Ce bond must be the active phase. Increased crystallinity decreases the number of exposed V–O–Ce bonds due to the lower surface-to-volume ratio, which accounts for catalyst deactivation.

Ascoop et al. [15] studied a WO_x–VO_x/SiO_2 catalyst and using isotopic labelling confirmed that in parallel to an oxidative dehydrogenation pathway (reaction 1), also reverse water gas shift reaction ($H_2 + CO_2 \leftrightarrow CO + H_2O$) and a direct, non-oxidative propane dehydrogenation reactions ($C_3H_8 \rightarrow C_3H_6 + H_2$) occur over the catalyst at 600 °C. According to their DFT calculations, C-H bond activation in propane is the rate-limiting reaction step, whereas catalyst re-oxidation (V^{3+} to V^{4+}) with CO_2 occurs much faster.

Turakulova et al. [16] observed that the interaction between supported VO_x and $Ce_{0.46}Zr_{0.54}O_2$ results in the formation of $CeVO_4$, which is the active phase responsible for propane ODH. The full oxidation of propane to CO_x is reported to be catalysed at the $CeZrO_2$ surface, whereas propene is formed over $CeVO_4$. The oxygen exchange properties of the catalyst play an essential role in the ODH reaction. Contrary to Ascoop et al. [15], Turakulova et al. report that re-oxidation of the active sites is the rate-limiting step of the process, which is associated with the redox properties of the $VO_x/Ce_{0.46}Zr_{0.54}O_2$ catalyst.

Nowicka et al. [17] studied propane-CO_2 ODH reaction over Pd/CeZrAlO_x catalysts and showed that over ceria-based catalysts, the reaction proceeds via the Mars van

Krevelen mechanism in parallel with the RWGS reaction. The high propene selectivity (95% at ~ 3% propane conversion) was attributed to the exclusive formation of selective oxide (O^{2-}) ions when CO_2 dissociates at the surface oxygen vacancy sites of CeO_2. The role of Pd is to enhance the reducibility and to accelerate the re-oxidation of the CeO_{2-x} surface. Strong catalyst deactivation was attributed to carbon accumulation which blocks the active sites and incomplete catalyst oxidation by CO_2.

Carbon materials with a high surface area and large pore volume have an increasing number of applications as catalyst supports and adsorbents [18–20]. They can be synthesized in a variety of morphologies (nanotubes, ordered mesoporous structures, etc.) and their surfaces can be functionalized with adatoms (V and N) or oxygen containing groups, giving rise to catalytic activity in many reactions, including oxidative dehydrogenation of propane [21–23].

Our common observation in many propane-CO_2 ODH studies is that catalytic tests were run at relatively high reaction temperatures (600–700 °C) in order to activate CO_2 and ensure reasonable conversions. Under such conditions, thermal (noncatalytic) reactions strongly contribute to the observed propane conversion and influence the distribution of reaction products [7, 15].

This work is focused on the systematic analysis of propane and CO_2 interaction with bulk and activated carbon (AC) supported VO_x, CeO_2 and $CeVO_4$ catalysts. Vanadia based materials are very often investigated catalysts in the oxidative dehydrogenation of parafines [1], whereas ceria is known for its reactivity towards CO_2 [24]. Consequently, these materials, as well as their mixed oxide phase ($CeVO_4$) were the subject of this investigation. Structural, redox, and chemical nature of the active phases were varied by changing their loading on the AC support and were correlated to activity, stability, and olefin selectivity in the propane-CO_2 ODH reaction.

2 Experimental

2.1 Synthesis of Catalysts

Bulk V_2O_5 was synthesised by calcination of vanadium acetyl-acetonate (Sigma Aldrich, purity 99%). Bulk $CeVO_4$ was synthesised by completely dissolving 92 mg of NH_4VO_3 (Sigma Aldrich, p.a.) in 65 ml of ultrapure water (resistivity of 18.2 MΩ, Elga Purelab Option-Q), while the solution was heated to 80 °C and stirred with a magnetic stirrer. To prevent water evaporation, the glass beaker was covered with a petri dish. Once dissolved, 1 drop of concentrated HNO_3 was added. In a separate glass beaker, 340 mg of $Ce(NO_3)_3 \times 6H_2O$ (Sigma Aldrich, purity 99%) was dissolved in 10 ml of ultrapure water. After complete dissolution, the prepared solutions were mixed, resulting in an instantaneous formation of a yellow–brown precipitate. The suspension was stirred at 80 °C for an additional 2 h. After cooling, filtering and washing 3 times with ultrapure water, the suspension was dried overnight at 70 °C in a laboratory drier. Pure CeO_2 was synthesised by dissolving 4.9 g of $Ce(NO_3)_3 \times 6H_2O$ (Sigma Aldrich, purity 99%) in 84 ml of ultrapure water. This solution was mixed with 140 ml of 0.1 M aqueous NaOH and stirred for 30 min. Afterwards, it was transferred to Teflon® lined autoclaves (~ 35 ml volume), which were placed into a laboratory drier preheated to 180 °C and kept at this temperature for 24 h. The precipitate was filtered, washed 3 times with ultrapure water, and dried overnight at 70 °C in a laboratory drier. All bulk catalysts were calcined 4 h at 600 °C (Nabertherm, model LT 9/11, heating ramp of 2 °C/min) in static air.

Synthesis of catalysts containing $CeVO_4$ (10–40 wt% $CeVO_4$) supported on activated carbon (AC) was similar to the one of bulk $CeVO_4$ with the following exceptions: 0.7 g of activated carbon, finely ground in an agate mortar, was added to the aqueous NH_4VO_3 solution. After filtration the samples were dried overnight at 70 °C. The VO_x (2–12 wt% vanadium) was deposited over AC by dissolving appropriate amounts of NH_4VO_3 in 10 ml of ultrapure water at 80 °C. Afterwards, 0.7 g of AC was added, stirred for another 2 h at room temperature, filtered and dried overnight at 70 °C in a laboratory drier. CeO_2 (7–17 wt% cerium) was deposited over AC by dissolving appropriate amounts of $Ce(NO_3)_3 \times 6H_2O$ in 1 ml ultrapure water. Afterwards, 0.7 g of AC was added, mixed for 2 h and dried overnight at 70 °C. All AC supported catalysts were calcined (4 h at 600 °C, 2 °C/min heating ramp) in a tubular oven (Carbolite, model HST 12/400) in Argon (20 l/h) to prevent AC oxidation. The $CeVO_4$ content in the $CeVO_4$/AC catalysts was selected so the actual content of vanadium or cerium in the $CeVO_4$ phase covered a similar range as in CeO_2/AC or VO_x/AC catalysts. Actual content of vanadium, cerium and $CeVO_4$ is shown in Table S1.

2.2 Characterisation and Catalytic Testing

XRD analyses were performed on a PANalytical X'pert PRO diffractometer using Cu Kα radiation ($\lambda = 0.15406$ nm) between 2theta angles of 10° and 80° with the step size of 0.034°. The BET specific surface area, total pore volume and average pore size were determined using N_2 adsorption/desorption isotherms at 77 K (Micromeritics, model TriStar II 3020). The samples were degassed before measurements using a SmartPrep degasser (Micromeritics) in a N_2 stream 1 h at 90 °C followed by 4 h at 180 °C. Actual vanadium, cerium and $CeVO_4$ contents were determined from the mass of oxidic residue remaining after complete oxidation of the AC support (TGA apparatus, model STA6000 by Perkin

Elmer) by heating the samples in air (25 ml/min) with a heating ramp of 10 °C/min to 800 °C. The carbon content, accumulated on the bulk catalyst during reaction was analysed by CHNS analytical technique (Series II CHNS analyser, model 2400 from Perkin Elmer).

Prior to TEM analysis, samples were dispersed in absolute ethanol and sonicated for 30 s, then directly transferred to Cu lacey carbon support grids. As prepared samples were analysed by 200 kV transmission electron microscope (TEM, JEM-2010F, Jeol Inc.) and by C_s-corrected (TEM, Titan Themis G^3, FEI Inc., equipped with CEOS CETCOR aberration corrector) operating at 300 kV. Amount of carbon deposited on the bulk unsupported catalysts during the catalytic reaction was analysed using CHNS elemental analyser (Perkin Elmer, model 2400).

Catalyst reduction with propane (C_3H_8-TPR) and oxidation with CO_2 (CO_2-TPO) was analysed in the Micromeritics Autochem 2920 apparatus. The powdered samples (100 mg) were positioned on a flock of quartz wool inside an U-shaped quartz reactor. The samples were pre-treated with He (Linde, purity 5.0) for 30 min at 300 °C, followed by cooling to 10 °C, switching to a 50% C_3H_8/He flow (10 ml/min) and heating to 600 °C with a 10 °C/min ramp. The samples were again cooled to 10 °C, and re-oxidation by CO_2 (Linde, purity 5.3) was started by increasing the temperature until 700 °C with a 10 °C/min ramp. The analytical protocol is shown in Fig. S1. Reaction products were monitored by mass spectrometry (model Thermostar®, Pfeiffer Vacuum) propane (m/z = 29), propene (m/z = 41), ethene and ethane (m/z = 27), methane (m/z = 15), water (m/z = 18), CO_2 (m/z = 44), He (m/z = 4) and H_2 (m/z = 2).

Transient interaction of bulk $CeVO_4$, CeO_2 and V_2O_5 with propane and CO_2 was analysed with Diffuse Reflectance Infrared Furrier Transformed Spectroscopy (DRIFTS) analysis (Perkin Elmer, model Frontier) equipped with DiffusIR cell from Pike Scientific. Approximately 10 mg of finely powdered sample was pre-treated in 20%O_2/He stream at 550 °C for 15 min. Afterwards, the sample was exposed to the following sequence of atmospheres: 20% O_2/He → 20% C_3H_8/He → 20% CO_2/He. Sample spectra were recorded continuously (4 s between scans) in the range between 500 and 4000 cm^{-1}, 8 accumulations per scan and spectral resolution of 4 cm^{-1}.

Raman analysis of the powdered catalysts was performed in the spectral range from 70 to 3700 cm^{-1} using Witec Alpha 300 spectrometer that employed green laser with excitation wavelength of 532 nm and resolution of 4 cm^{-1} at 30 mW laser power.

Catalytic experiments were performed in a PID Eng&Tech reactor system using a quartz tubular reactor (10 mm I.D.). The powdered catalyst (300 mg) was positioned between two flocks of quartz wool. Reaction temperature was measured with a K-type thermocouple, which was covered by a quartz sleeve, thus minimising the heated volume inside the reactor above the catalyst bed. A quartz rod was used to minimise the reactor volume after the catalyst bed. This reduced the occurrence of thermal, non-catalytic reactions (verified with a blank experiment which showed < 0.5% propane conversion at 550 °C. Before the catalytic reaction, the catalyst was heated using a heating ramp of 10 °C/min in a flow of CO_2 (Linde, purity 5.3) and He (Linde, purity 5.0) with a flowrate of 10 ml/min each, until reaching the reaction temperature of 550 °C. Afterwards, the propane flow (Linde, purity 3.5, 10 ml/min) was added and 15 min were allowed before starting the GC analysis to allow for stabilization of gas concentrations. Agilent 7890A gas chromatograph (equipped with Molesieve 5A and Poraplot Q columns and two TCD detectors) was used for qualitative and quantitative analysis of gas stream. The carbon mass balances were in all cases between 85 and 104%. Operation in kinetic regime was ensured by plotting the propane reaction rate versus progressively increasing C_3H_8/CO_2/He flowrate over a constant mass of catalyst (Fig. S2). Details on calculation of propane conversion and product selectivities are provided in the Supplementary information.

3 Results

3.1 Catalytic Activity of Bulk CeO_2, V_2O_5 and $CeVO_4$

Catalytic performance of all materials during propane-CO_2 ODH reaction is summarized in Tables 1 and 2.

Main reaction product over bulk CeO_2 was CO, along with CH_4 and H_2 (71, 10 and 13% selectivity, respectively). The olefin selectivity was low (12% for propene and 4% for ethene).

The bulk V_2O_5 deactivated quickly: the initial propane conversion of 9.5% stabilised at 3.2% after 240 min TOS (Fig. 1a). Also, C_3H_6 selectivity decreased from 27 to 0% (Table 1 and Fig. 1b) and CO dropped to zero in 140 min (not shown). Contrary, selectivities for H_2 and CH_4 increased slowly during the experiment from 9 to 25% and 31 to 61%, respectively. This transient behaviour of the V_2O_5 catalyst indicates drastic changes in contribution of several possible reaction pathways occurring during propane-CO_2 ODH reaction: (i) oxidative dehydrogenation with participation of lattice oxygen producing propene and water, (ii) oxidative dehydrogenation with CO_2 acting as the oxidant, producing propene, CO and water (iii) total oxidation of propane to CO_x and water, (iv) nonoxidative dehydrogenation pathway producing propene and hydrogen and (v) propane cracking to CH_4, H_2 and carbon which deposits over the catalyst's surface (reactions 1–4). The relevance of these reactions will be discussed in detail in the following sections.

Table 1 Initial propane conversion, propane reaction rate, propene selectivity and propene yield at 550 °C. Numbers in parentheses represent values after 240 min of reaction

Catalyst sample	C_3H_8 conversion (%)	Propane reaction rate, μmol/g_{cat} min	C_3H_6 selectivity (%)	C_3H_6 yield (%)
AC	2 (2)	30	28 (19)	0.6 (0.4)
CeO_2	5.6 (4.1)	84	10 (12)	0.6 (0.5)
V_2O_5	9.4 (3.2)	141	27 (0)	2.5 (0)
$CeVO_4$	4.3 (3.6)	65	28 (26)	1.2 (0.9)
$2VO_x$/AC	12.3 (5.8)	185	28 (40)	3.4 (2.3)
$5VO_x$/AC	10.5 (6.2)	155	37 (51)	3.9 (3.2)
$12VO_x$/AC	13.8 (7.7)	207	36 (44)	4.9 (3.4)
$7CeO_2$/AC	12.4 (4.8)	184	17 (34)	2.1 (1.6)
$12CeO_2$/AC	9.7 (3)	145	27 (62)	2.6 (1.9)
$17CeO_2$/AC	10.1 (6.4)	152	23 (28)	2.3 (1.8)
10 $CeVO_4$/AC	7 (6)	105	41 (29)	2.9 (1.7)
15 $CeVO_4$/AC	9.3 (7)	140	42 (43)	3.9 (3)
20 $CeVO_4$/AC	11.2 (8.5)	166	49 (57)	5.5 (4.8)
30 $CeVO_4$/AC	15.3 (10.1)	230	42 (49)	6.4 (4.9)
40 $CeVO_4$/AC	12.9 (7)	194	47 (62)	6.1 (4.3)

Reaction conditions: 33% C_3H_8, 33% CO_2, 34% He, T = 550 °C, WHSV = 6000 ml/g_{cat} h.

Table 2 Product selectivity of AC supported catalysts after 240 min of reaction. See Supplementary Information file for details on calculation of these values

Sample	Selectivity (%)				
	C_3H_6	C_2H_4	CH_4	CO	H_2
$2VO_x$/AC	40	1	6	50	10
$5VO_x$/AC	51	2	6	43	10
$12VO_x$/AC	44	1	5	41	8
10$CeVO_4$/AC	29	0	5	59	18
15$CeVO_4$/AC	43	1	5	37	9
20$CeVO_4$/AC	57	4	11	22	9
30$CeVO_4$/AC	49	1	4	35	11
40$CeVO_4$/AC	62	0	5	28	7
$7CeO_2$/AC	34	2	11	50	8
$12CeO_2$/AC	62	3	19	14	13
$17CeO_2$/AC	28	2	9	56	6

$$C_3H_8 \rightarrow C_2H_4 + CH_4 \quad (2)$$

$$C_3H_8 \rightarrow C_3H_6 + H_2 \quad (3)$$

$$C_2H_4 \rightarrow CH_4 + C \quad (4)$$

Activity of bulk $CeVO_4$ was stable, as well as selectivity for all reaction products: C_3H_6, CH_4, H_2 and C_2H_4 at 25, 31, 26 and 18%, respectively. No CO was formed, which indicates the lattice oxygen or CO_2 participation (Reaction 1) and RWGS reaction ($CO_2 + H_2 \leftrightarrow H_2O + CO$) are not occurring over this catalyst. The non-oxidative dehydrogenation and propane/propene cracking dominate the reaction product distribution over bulk $CeVO_4$. Results of a blank experiment (Fig. S3) show that no conversion is taking place at 550 °C in the empty reactor. This confirms the non-oxidative dehydrogenation reaction is a consequence $CeVO_4$.

3.2 Catalytic Activity of AC Supported Catalysts

3.2.1 CeO_2/AC Catalysts

Propane conversions and propene selectivities were notably higher over CeO_2/AC catalysts compared to bulk CeO_2 (Table 1). A notable (~ 50%) decrease in propane conversion in the initial 60 min of reaction for $7CeO_2$/AC (Fig. 2a) was accompanied by an increase in propene selectivity.

3.2.2 VO_x/AC Catalysts

Catalytic stability of VO_x/AC catalysts is notably improved compared to bulk V_2O_5 (Table 1, Figs. 1A and 2A). Propene selectivities ranged between 40 and 51% and were marginally influenced by vanadium content, which was varied between 2 to 12 wt%. Selectivities for CO were between 41 and 50%, for H_2 ranged between 8 and 10%, for CH_4 between 5–6% and for C_2H_4 between 1–2% (Table 2). Contrary to the complete loss of propene selectivity over bulk V_2O_5, the propene selectivity over VO_x/AC catalysts was stable during the 240 min of reaction (Fig. 2b). This indicates markedly different catalytic behaviour of supported vanadium species compared to bulk V_2O_5.

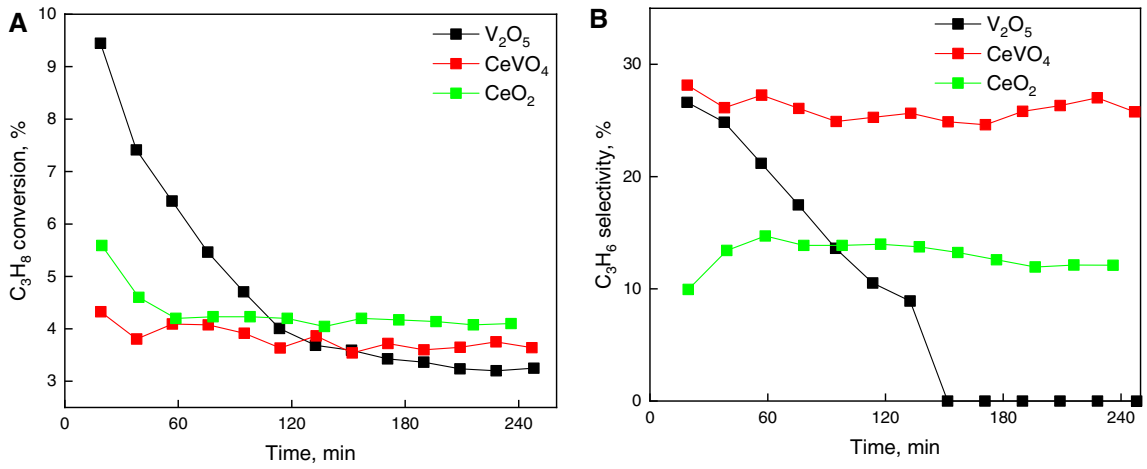

Fig. 1 Propane conversion (**a**) and propene selectivity (**b**) as a function of TOS over bulk V_2O_5, $CeVO_4$ and CeO_2 catalysts during propane-CO_2 ODH reaction. Please refer to online version of this manuscript for colour figure

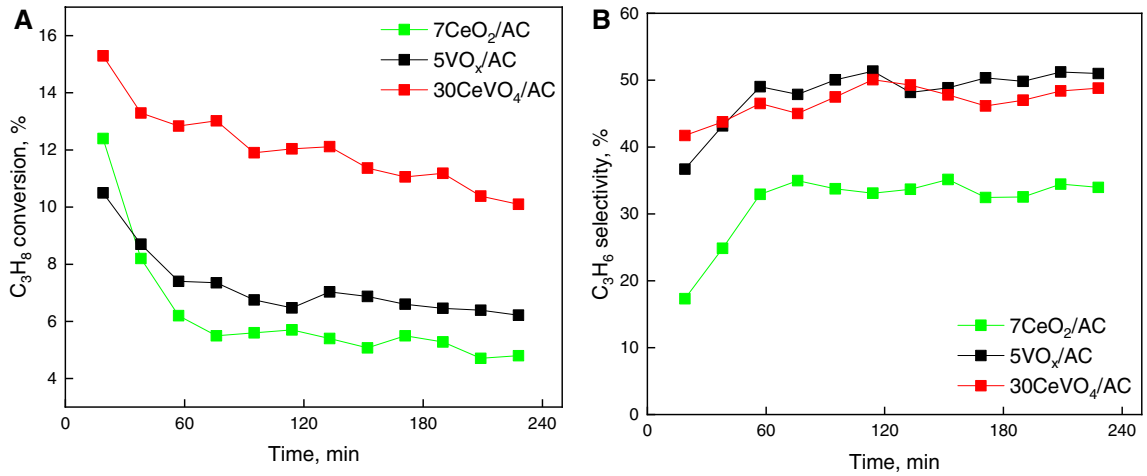

Fig. 2 Propane conversion (**a**) and propene selectivity (**b**) as a function of TOS over $7CeO_2$/AC, $5VO_x$/AC and $30CeVO_4$/AC catalysts during propane-CO_2 ODH reaction. Please refer to online version of this manuscript for colour figure

3.2.3 $CeVO_4$/AC Catalysts

Testing of $CeVO_4$/AC catalysts revealed a positive correlation between $CeVO_4$ content and catalytic activity, as well as propene selectivity. The $30CeVO_4$/AC sample achieved 11.4% propane conversion and 57% propene selectivity at 60 min TOS (Table 1 and Fig. 2). This is clearly superior compared to all tested bulk and supported VO_x, CeO_2 and $CeVO_4$ materials. For all $CeVO_4$/AC catalysts, a slow continuous deactivation was observed with time on stream. Selectivities for CO ranged between 22 and 59%, H_2 ranged between 8 and 18%, for CH_4 between 5 and 11% and for C_2H_4 up to 4% (Table 2).

Catalytic propane dehydrogenation reaction often suffers from poor stability, which is usually caused by carbon build-up on the catalyst, which blocks the active sites [6]. A long-term catalytic test was performed on the $20CeVO_4$/AC catalyst (Fig. 3). Continuous deactivation was observed in the first 30 h of reaction; the catalyst lost 71% of its initial activity (based on the drop of propane conversion). Catalyst deactivation was accompanied by a slow rise in propene, CH_4, C_2H_4 and H_2 selectivities (Fig. 3), as well as decrease of CO selectivity (not shown). This indicates a slow transition from an oxidative propane-CO_2 to a non-oxidative propane dehydrogenation pathway. Finally, conversions of propane and CO_2 stabilised at 3% each. Very similar behaviour was observed over $Pd/CeZrAlO_x$ catalysts during propane-CO_2 ODH reaction at 600 °C by Nowicka et al.[17]

An important aspect for discussion of catalytic performance of AC supported catalysts is experimental verification

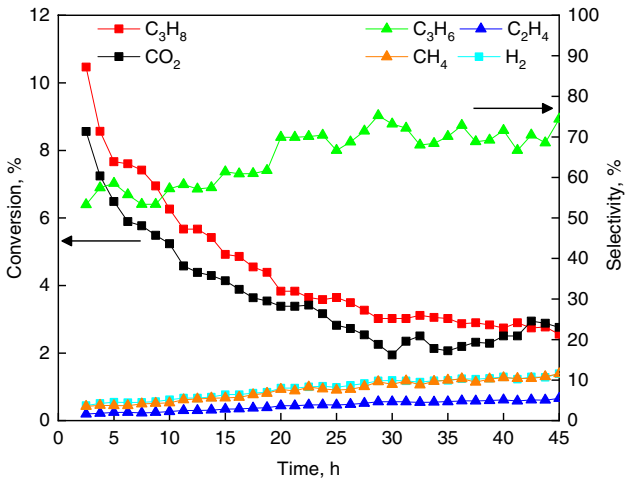

Fig. 3 Catalytic performance of 20$CeVO_4$/AC catalyst during the propane-CO_2 ODH stability test. Please refer to online version of this manuscript for colour figure

that support gasification does not contribute to measured reaction products. Under simulated reaction conditions (4 h at 550 °C in a 30 ml/min total flow consisting of 33% C_3H_8, 33% CO_2 and 33% He) inside a thermogravimetric apparatus, the mass of 20$CeVO_4$/AC catalyst increased by 0.58 wt. % (Fig. S4A). This experiment confirmed a small amount of carbon was deposited on the catalyst during the 4 h of reaction. Additionally, the TGA-TPO experiment of fresh and spent 20$CeVO_4$/AC catalysts after 45 h of reaction showed the weight fraction of carbon in the sample increased by 0.62 wt% (Fig. S4B). These two experiments revealed no gasification of the AC support during catalytic reaction and that carbon accumulation on the catalyst is low and occurs mainly in the initial 4 h of reaction. Spent bulk catalysts after 4 h of propane-CO_2 ODH reaction contain 1.6, 1.4 and 1.4 wt% of carbon for $CeVO_4$, V_2O_5 and CeO_2, respectively.

Propene selectivity at comparable propane conversions is shown in Fig. S5 for all catalysts, which revealed increasing selectivity in the following order: $CeVO_4 > V_2O_5 > CeO_2$.

3.3 Catalyst Characterisation

3.3.1 N_2 Physisorption and XRD Analysis

Morphological properties analysed by N_2 physisorption technique are compiled in Table 2. The V_2O_5 and $CeVO_4$ are mesoporous with total low pore volumes and BET specific surfaces, whereas specific surface area of CeO_2 is much higher. After 4 h of reaction, the specific surface area of CeO_2 drops by about 50%, whereas changes for V_2O_5 and $CeVO_4$ were much smaller. The specific surface area and pore volume of supported catalysts are dominated by the microporous activated carbon support. With increasing content of the active phase (VO_x, CeO_2 or $CeVO_4$), a continuous decrease of specific surface area and pore volume are observed, which is in line with a progressively larger contribution from the deposited oxides.

XRD analysis was performed on the fresh and spent catalysts (Figs. 4, 5 and S6). In bulk $CeVO_4$ and $CeVO_4$/AC samples (Fig. 4a), only a $CeVO_4$ phase (PDF 00-012-0757) was observed. No diffraction lines of crystalline CeO_2, V_2O_5 or V_2O_3 could be identified. The Scherrer equation was applied and the average scattering domain size of the $CeVO_4$ crystallites was calculated based on its most intense diffraction line

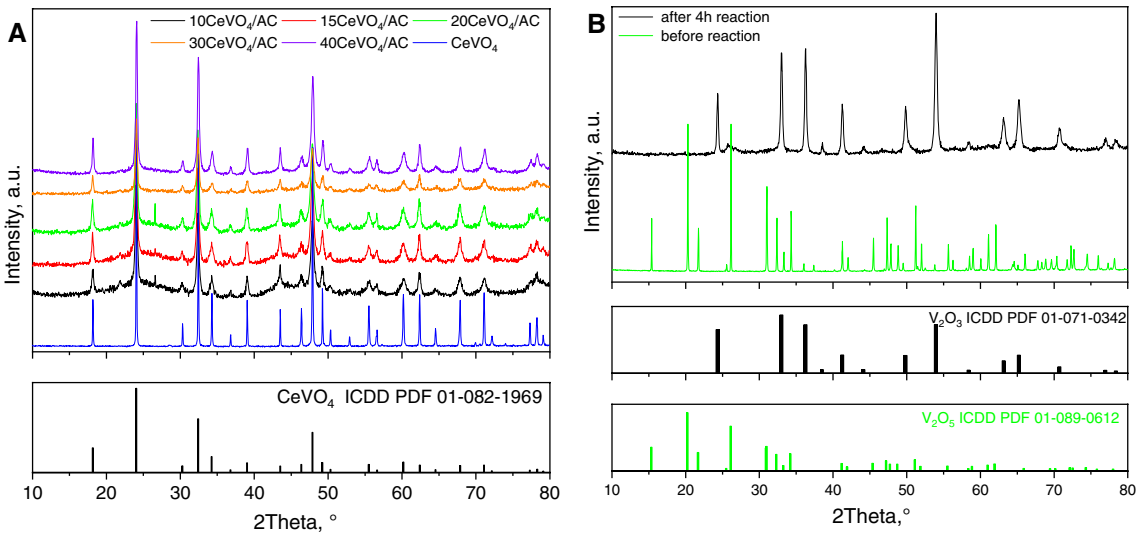

Fig. 4 **a** XRD patterns of fresh bulk $CeVO_4$ and $CeVO_4$/AC catalysts and **b** V_2O_5 before and after 4 h of propane-CO_2 ODH reaction. Please refer to online version of this manuscript for colour figure

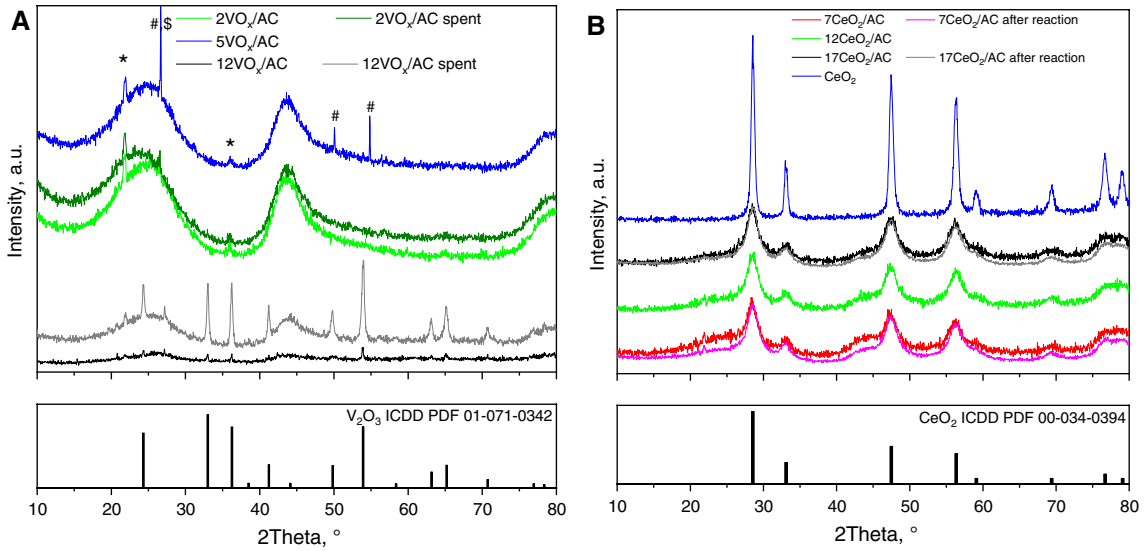

Fig. 5 **a** XRD patterns of VO_x/AC and **b** CeO_2/AC catalysts before and after 4 h propane-CO_2 ODH tests. Please refer to online version of this manuscript for colour figure

at 2θ = 24°. For bulk $CeVO_4$, the calculated average scattering domain size was 80 nm, whereas for the AC supported $CeVO_4$ catalysts this value was lower and increased from 25 nm in the 10$CeVO_4$/AC to 33 nm in the 40$CeVO_4$/AC sample. These results indicate the AC supports limits the crystal growth of the $CeVO_4$. The XRD results of 20$CeVO_4$/AC sample before, and after 4 and 45 h of propane-CO_2 ODH reaction (Fig. S6) showed no structural changes in the $CeVO_4$ and negligible sintering since the average crystallite size measured 24, 25 and 26 nm, respectively. The average pore diameter of AC supported catalysts is below 2 nm, which indicates that $CeVO_4$ crystallites observed by XRD, which are more than an order of magnitude larger, reside in the interparticle voids of the AC support.

XRD analysis of bulk V_2O_5 sample before and after propane-CO_2 ODH reaction (Fig. 4b) shows that the initially present V_2O_5 phase (PDF 01-089-0612), is reduced and quantitatively transformed to V_2O_3 (PDF 01-071-0342).

Results for the VO_x/AC samples before and after catalytic tests are shown in Fig. 5a. The broad reflection peaks between 20°–30° and 40°–50° are visible on all samples and originate from activated carbon. The diffraction lines at 21.8°, 26.6° and 35.8° can be ascribed to SiO_2 cristobalite*, quartz[#] and graphite[$] (PDF 01-089-3435, 01-085-1780 and 01-075-2078, respectively). These crystalline phases are present in the pristine activated carbon. The amount of SiO_2 in the AC was determined to be 1.1 wt% (thermogravimetric heating of pristine AC sample in air, followed by SEM-EDXS analysis of inorganic, non-combustible residue). No diffraction peaks from vanadium containing crystalline phases could be identified in the 2VO_x/AC and 5VO_x/AC samples.

In the fresh 12VO_x/AC sample weak diffraction lines at characteristic positions for V_2O_3 became apparent (PDF 01-071-0342). Formation of V_2O_3 is triggered by sample calcination in argon (see experimental section). The intensity of diffraction lines belonging to V_2O_3 increased after 4 h of reaction, revealing its sintering.

Figure 5b shows XRD results of bulk and supported CeO_2/AC catalysts. In all samples, only diffraction lines belonging to CeO_2 (PDF 00-034-0394) were identified. Average crystallite size in bulk CeO_2 was 15 nm (calculated by the Scherrer equation).

Broad diffraction lines characteristic of CeO_2 were identified in the CeO_2/AC catalysts with the average crystallite size of 4 nm which did not change with increasing CeO_2 content from 7 to 17 wt%. Negligible growth of CeO_2 crystallites occurred during the catalytic reaction, as average crystallite size of CeO_2 after reaction increased to 5 nm (Table 3). The AC support efficiently prevented sintering of the deposited CeO_2 during the reaction.

3.3.2 TEM Analysis

To explore the rapid drop of the catalytic performance, the 20$CeVO_4$/AC sample was analysed before and after 45 h of reaction (Fig. 6). In the fresh sample, the individual $CeVO_4$ crystals are agglomerated in larger clusters, deposited on the outer surface of AC support. The average $CeVO_4$ particle size measured 24 nm (Fig. S7A), which is in line with XRD estimation (Table 2). Selective area electron diffraction (SAED) pattern analysis confirmed the presence of a crystalline $CeVO_4$ phase only (Fig. 6, inset). The $CeVO_4$ crystallites have a plate-like polyhedral shape

Table 3 Specific surface area, total pore volume, average pore diameter and average crystallite size of fresh AC supported and bulk catalysts

Sample	BET (m^2/g)	Total pore volume (cm^3/g)	Average pore diameter (nm)	Crystallite site[a] (nm)
V_2O_5	10 (9)	0.05 (0.04)	19.2 (20.2)	101
CeO_2	74 (39)	0.15 (0.08)	7.8 (8)	15
$CeVO_4$	5 (5)	0.01 (0.01)	10.4 (9.7)	80
AC	1455	0.71	< 2	–
10$CeVO_4$/AC	1446	0.76	< 2	25
15$CeVO_4$/AC	1133	0.60	< 2	26
20$CeVO_4$/AC	1138 (1105)	0.62 (0.54)	< 2	24 (25)
30$CeVO_4$/AC	1026	0.54	< 2	32
40$CeVO_4$/AC	826	0.45	< 2	33
2VO_x/AC	1462	0.74	< 2	NA
5VO_x/AC	1254	0.66	< 2	NA
12VO_x/AC	1007	0.53	< 2	NA (22)
7CeO_2/AC	1236	0.64	< 2	4 (5)
12CeO_2/AC	1138	0.59	< 2	4
17CeO_2/AC	1066	0.55	< 2	4 (5)

Values in parentheses indicate values obtained for catalysts after the 4 h of propane-CO_2 ODH catalytic test.

[a]Calculated from XRD data. NA: No diffraction lines of vanadium containing phases are distinguishable in the catalysts.

and well developed 3D morphology (bulges and cavities) and are additionally covered with a thin (1–2 nm) amorphous layer of $CeVO_4$.

After the 45 h catalytic test, negligible increase in $CeVO_4$ crystallite size could be measured (Fig. S7B), which is in line with the XRD analysis. However, two changes were observed on the large majority of visualized $CeVO_4$ crystallites: (i) the amorphous layer present in the fresh sample was absent and (ii) $CeVO_4$ crystallites were covered with 2–3 atomic layers of amorphous carbon, encapsulating the surface of the $CeVO_4$ NPs. More details on the characterization of the amorphous $CeVO_4$ layer and carbon layers are provided in the supplementary information and Figs. S8–S10.

In order to visualize and analyse the catalytically active phase in the 5VO_x/AC catalyst, TEM-SAED analyses were performed (Fig. 7). It was observed that the activated carbon was covered by cubic crystallites measuring 3–10 nm in size. Selective area electron diffraction (SAED) pattern analysis identified these crystals as a cubic vanadium carbide phase (Fig. 7d). No vanadium oxides (crystalline V_2O_3 or V_2O_5) could be identified.

3.3.3 Temperature Programmed Reduction with Propane (C_3H_8-TPR)

Catalyst interaction with propane (Fig. 8) and CO_2 (Fig. 9) was tested according to the protocol shown in Fig. S1. These experiments investigated: (a) the ability of lattice oxygen to react with propane, (b) the re-oxidation of the reduced catalyst by CO_2, and how these processes are influenced by the morphology of the VC, VO_x, CeO_2 and $CeVO_4$ phases. During the C_3H_8-TPR experiments, CO_x and water were identified in parallel to propane conversion (drop of propane signal in Fig. 8), indicating participation of lattice oxygen in the propane conversion.

Propane signal as a function of temperature over CeO_2 containing catalysts is shown in Fig. 8a. Several broad, low-intensity bands are apparent between 150 and 500 °C in CeO_2/AC samples, which is absent in bulk CeO_2. These are likely related to propane reacting with coordinatively unsaturated surface lattice oxygen, which are more reactive in 4 nm CeO_2 crystallites (present in all CeO_2/AC samples), compared to bulk CeO_2 (15 nm). Propane conversion lights-off between 495 and 508 °C for AC supported samples, whereas a higher temperature (530 °C) is required for propane activation over bulk CeO_2.

Bulk $CeVO_4$ shows negligible activity for reduction by propane up to 600 °C (black line in Fig. 8b). However, propane is able to reduce the $CeVO_4$/AC samples already between 480 and 505 °C, producing propene and water.

Over bulk V_2O_5, propane is oxidized extensively in the low temperature region between 350 and 500 °C producing propene and water. These results are consistent with the oxidative dehydrogenation pathway involving lattice oxygen and reduction of V_2O_5 to V_2O_3. The second propane consumption signal between 500 and 600 °C produces methane and especially hydrogen. This is consistent with catalytic tests at TOS > 140 min (Fig. 1). Propane cracking inevitably produces carbon deposition, but this could not be analysed. The VO_x/AC catalysts containing either only VC (2VO_x/AC and 5VO_x/AC) or a combination of VC and V_2O_3 (12VO_x/AC) are starting to decompose propane at about 485 °C. In all cases, propane conversion produces propene and hydrogen (Fig. 8c).

In all analysed samples, higher propane conversion during C_3H_8-TPR experiments (Fig. 8) generally correlates with higher catalytic activity (Table 1).

3.3.4 Temperature Programmed Oxidation with CO_2 (CO_2-TPO)

In situ oxidation experiments with CO_2 were performed on the catalysts previously exposed to the C_3H_8-TPR protocol (Fig. S1). During CO_2-TPO, CO_2 is dissociated over the catalyst to CO and O. The latter oxidizes the catalyst and

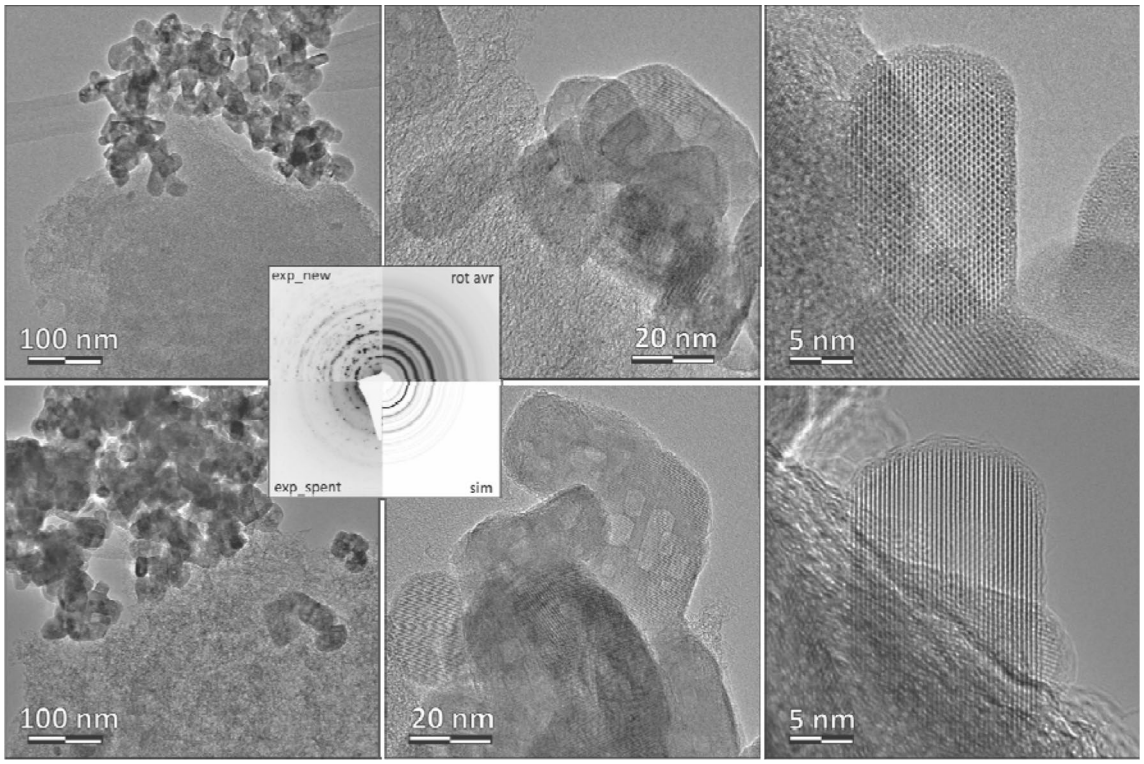

Fig. 6 TEM micrographs of 20 $CeVO_4$/AC catalyst before (upper row) and after (lower row) 45 h propane-CO_2 ODH test. SAED simulation (inset) was calculated using crystal structure data for tetragonal $CeVO_4$ (SG141, I41/amd) [25]

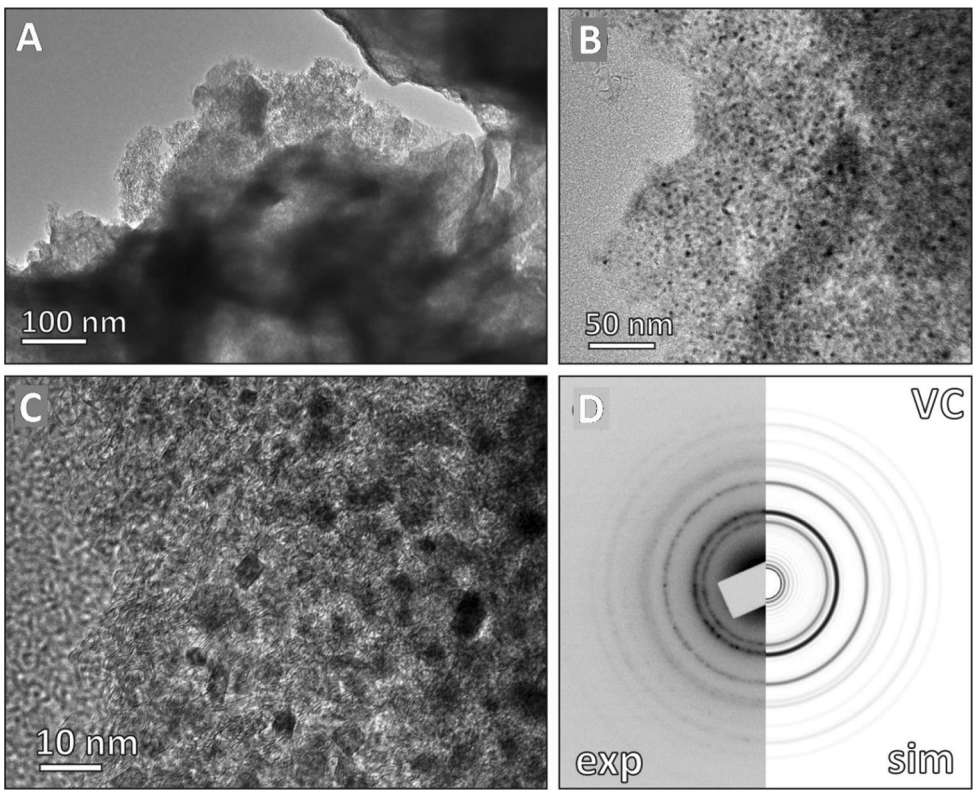

Fig. 7 TEM micrographs of fresh 5VO_x/AC catalyst at different magnifications (**a**–**c**); comparison of experimental and simulated SAED for cubic VC (**d**)

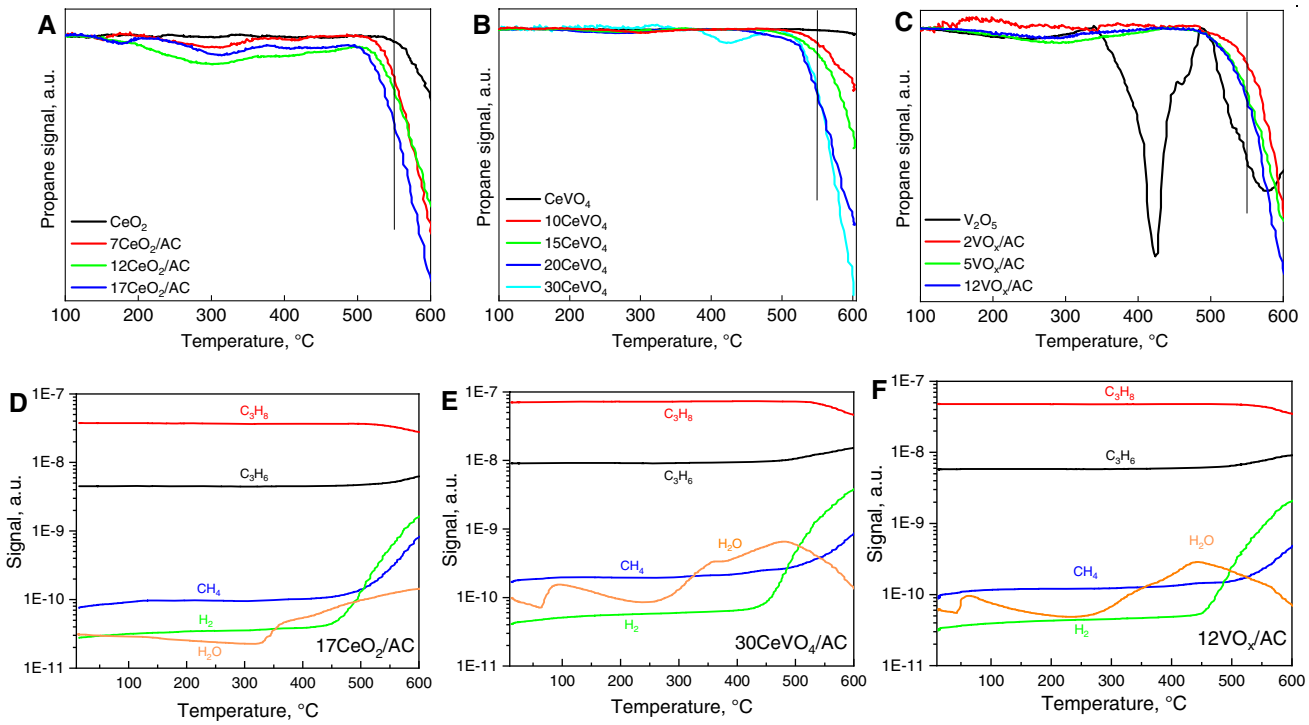

Fig. 8 The MS signal of propane during C_3H_8-TPR experiments over: **a** CeO_2 and CeO_2/AC; **b** $CeVO_4$ and $CeVO_4$/AC and **c** V_2O_5 and VO_x/AC catalysts. Vertical lines at 550 °C represent the propane-CO_2 ODH reaction temperature. **d–f** show MS signals of C_3H_8, C_3H_6, H_2, H_2O and CH_4 obtained over 17CeO_2/AC, 30$CeVO_4$/AC and 12VO_x/AC catalysts during C_3H_8-TPR, respectively. Please refer to online version of this manuscript for colour figure

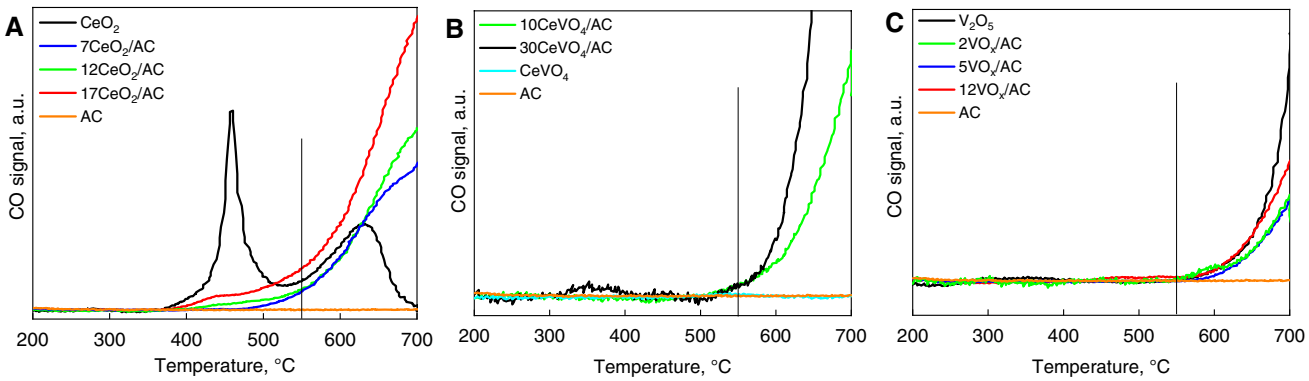

Fig. 9 CO signal measured during CO_2-TPO experiments over: **a** CeO_{2-x} and CeO_{2-x}/AC; **b** $CeVO_4$ and $CeVO_4$/AC and **c** V_2O_5 and VO_x/AC catalysts. Vertical lines at 550 °C represent the propane-CO_2 ODH reaction temperature. Please refer to online version of this manuscript for colour figure

CO desorbs. CO desorption profiles over different catalysts are shown in Fig. 9.

The re-oxidation of bulk CeO_{2-x} by CO_2 took place with appearance of two intense CO peaks centred at 460 and 620 °C (Fig. 9a). On the other hand, the re-oxidation of CeO_{2-x}/AC samples was initiated at between 400 and 450 °C with a slow, continuous rise of the CO signal until the final temperature of 700 °C was reached. This reveals very different dynamics of CeO_2 oxidation which is strongly related to the size of CeO_2 crystallites.

Bulk $CeVO_4$ does not react with CO_2 up to 700 °C (Fig. 9b), which is in line with inertness of this sample during C_3H_8-TPR and catalytic experiment showing no CO among reaction products. Over $CeVO_4$/AC catalysts, CO starts to appear at 500 °C and its amount continuously increases with increasing $CeVO_4$ loading.

Oxidation of bulk V_2O_3 (V_2O_5 catalyst after C_3H_8-TPR) and VO_x/AC catalysts with CO_2 was initiated at 570 °C (Fig. 9c), which reveals that at the reaction temperature of 550 °C, V_2O_3 cannot be re-oxidized with CO_2. This is in line with results of Ascoop et al. [15] who report that oxidation of WO_x–VO_x/SiO_2 catalysts with CO_2 at 600 °C can only transform V^{3+} to V^{4+}. Also, the VC phase is inert towards CO_2 at 550 °C.

The C_3H_8-TPR and CO_2-TPO results revealed that the reduction and re-oxidation of CeO_2, and $CeVO_4$ phases are strongly dependent on their morphology. Smaller CeO_2 crystals (4 nm) in CeO_2/AC are more readily reduced by propane compared to bulk CeO_2 (15 nm), whereas during re-oxidation by CO_2, the situation is reversed. Both processes are possible at 550 °C, which was also the temperature during propane-CO_2 ODH reaction.

The $CeVO_4$/AC samples can be reduced by propane and oxidized by CO_2 at 550 °C. This ability is absent in bulk $CeVO_4$, which has negligible activity for propane and CO_2 activation.

In the case of VO_x/AC catalysts, the vanadium containing phase depends on the vanadium content (V_2O_5 in bulk sample, VC in 2VO_x/AC and 5VO_x/AC and a mixture of V_2O_3 and vanadium carbide in 12 VO_x/AC sample). All VO_x/AC and V_2O_5 samples can dehydrogenate propane: bulk V_2O_5 already at 350 °C through the oxidative dehydrogenation pathway with lattice oxygen participation, whereas the crystalline VC is active above 485 °C through a non-oxidative pathway. Re-oxidation with CO_2 takes place above 570 °C.

3.3.5 Time Resolved Isothermal DRIFTS Experiments

Transient behaviour of CeO_2, $CeVO_4$ and V_2O_5 during isothermal reduction with propane and re-oxidation with CO_2 was investigated with an in situ DRIFTS analysis at 550 °C (Figs. 10, 11 and S11–S17). Only bulk oxides were analysed due to the black colour and total absorbance of all AC supported catalysts. No interaction of propane or CO_2 with $CeVO_4$ was observed and these results are consequently not shown.

Exposure of CeO_2 to propane (Fig. 10a) showed instantaneous formation of CO and CO_2 which decayed slowly with prolonging TOS. Also, a rapid increase of the broad polydentate carbonate bands (1454 cm^{-1}) was observed (Fig. S12A) [26, 27].

Exposure of reduced CeO_{2-x} to CO_2 (Figs. 10b, S13 and S14) leads to a fast increase of two broad polydentate carbonate bands centred at 1454 and 1350 cm^{-1} (Fig. S14A). These carbonates are observed regularly over ceria and are thermally very stable, as bands remain stable during the re-oxidation experiment. Also, instantaneous formation of CO is observed; it goes through a maximum and slowly starts to decline after 300 s of CO_2 exposure. This confirms CO_2 dissociation and oxygen vacancy replenishment, leading to oxidation of CeO_{2-x}. Existence of the band at 1765 cm^{-1} (CO adsorbed on reduced Ce^{3+} sites [28]) after 10 min of oxidation at 550 °C (Fig. S14A) suggests oxidation of CeO_{2-x} with CO_2 does not proceed to completion.

Upon exposure of V_2O_5 to propane (Figs. 11a, S15 and S16), the V=O vibration overtones at 2005 and 1969 cm^{-1} diminish after 53 s, indicating surface reduction [29]. In parallel to propane introduction, the CO_2 signal (2340 cm^{-1}) lights off, goes through a maximum at 135 s

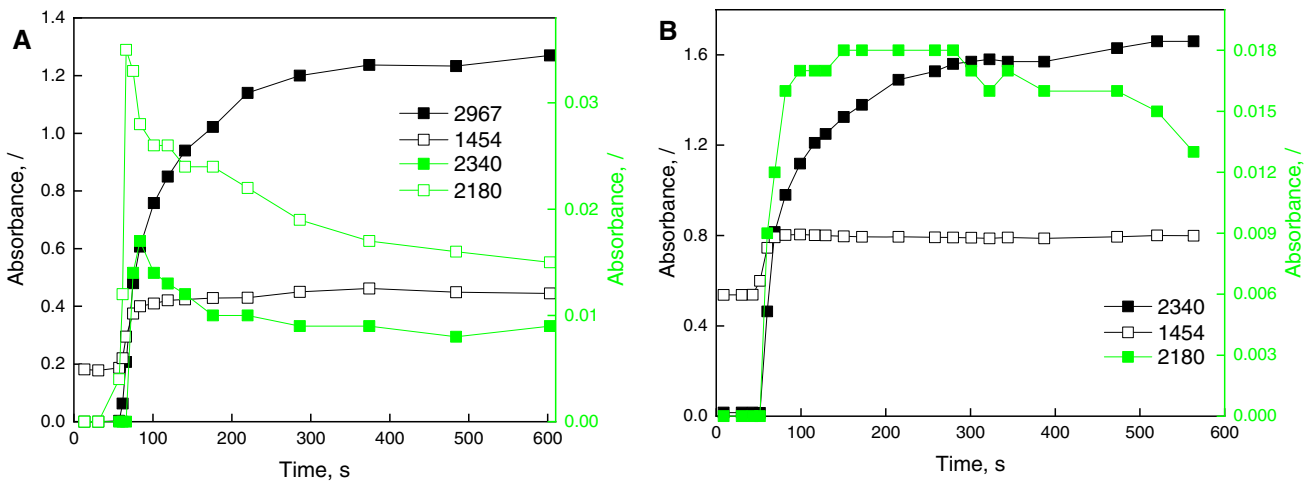

Fig. 10 **a** Reduction of CeO_2 with propane and time resolved signal intensity changes for propane (2967 cm^{-1}), CO_2 (2340 cm^{-1}), CO (2180 cm^{-1}), and carbonates (1454 cm^{-1}). **b** Re-oxidation of CeO_{2-x} with CO_2 and time resolved signal intensity changes of CO_2 (2340 cm^{-1}), CO (2180 cm^{-1}), and carbonates (1454 cm^{-1}). Please refer to online version of this manuscript for colour figure

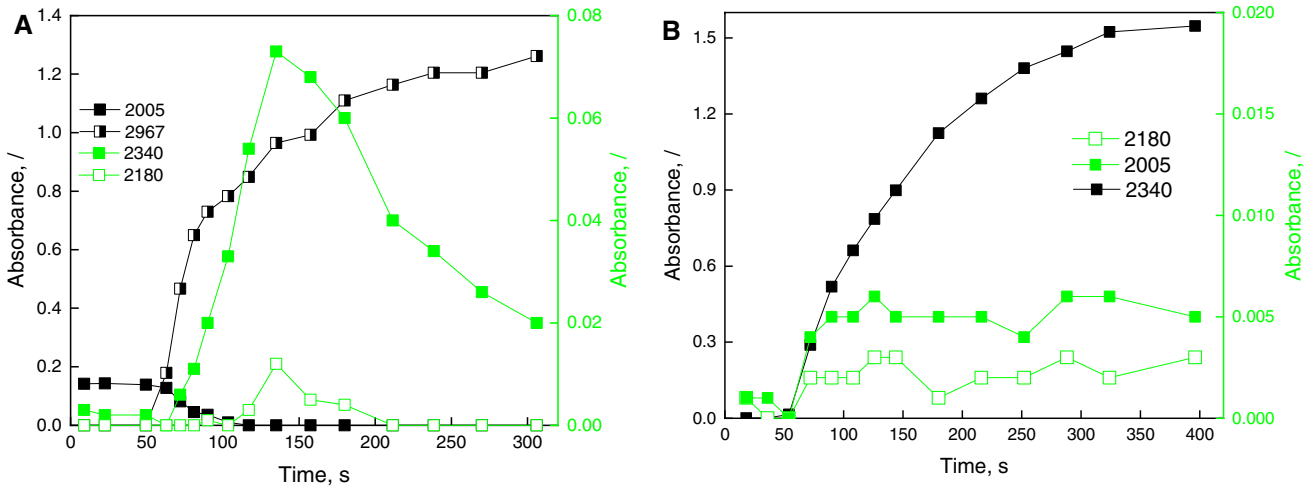

Fig. 11 A) Reduction of V_2O_5 with propane and time resolved signal intensity changes for propane (2967 cm^{-1}), CO_2 (2340 cm^{-1}), CO (2180 cm^{-1}), and V–O overtones (2005 cm^{-1}). B) Re-oxidation of V_2O_3 with CO_2 and temporal signal intensity changes of CO_2 (2340 cm^{-1}), CO (2180 cm^{-1}), V–O overtone (2005 cm^{-1}). Please refer to online version of this manuscript for colour figure

and declines slowly. Formation of gas phase CO (characteristic band at 2180 cm^{-1}) is much smaller compared to CO_2 and appears only after the surface V=O overtone signal disappears at 100 s. This time-resolved experiment reveals the oxidation of propane to CO is possible only in the presence of a partly reduced surface, most likely containing V^{4+}. On the reduced V_2O_3 sample, the envelope of signals between 1300 and 1550 cm^{-1} appears (Fig. S16A), which belong to gas phase propane; no carbonates are formed. Absence of bands above 1600 cm^{-1} indicates no carboxylates or bicarbonates are formed.

Re-oxidation of V_2O_3 with CO_2 occurs only marginally, since only about 3% of initial V=O band intensity was achieved after 400 s of oxidation, Fig. 11b, S17).

To summarize, time resolved DRIFTS experiments showed that reduction of CeO_2 with propane at 550 °C is fast, and that instantaneous surface population with polydentate carbonates takes place. Re-oxidation with CO_2 is substantial, but does not proceed to completion. This suggests the working state of the CeO_2 catalyst during the propane-CO_2 reaction is partly reduced.

Reduction of V_2O_5 is slower (CO_2 peak intensity is reached 60 s after propane introduction, compared to 5 s for CeO_2), re-oxidation by CO_2 is negligible. This suggests a slow irreversible transformation of initially present V_2O_5 into V_2O_3. Also, the inability of V_2O_5 and V_2O_3 to dissociate CO_2 shows the crucial role of lattice oxygen (nucleophilic O^{2-} species) for enabling the oxidative dehydrogenation reaction pathway for propene formation. These findings are in line with catalytic tests (stable activity and low propene selectivity over CeO_2, compared to fast deactivation and total loss of propene selectivity over V_2O_5).

3.3.6 Raman Analysis

In the fresh and spent $2VO_x$/AC and $5VO_x$/AC catalysts, no signal below 1000 cm^{-1} is visible (Fig. 12a). This is due to the absence of V–O bonds in these samples and shows that only vanadium carbide (VC) is present [30]. Also, the VC phase is resistant towards oxidation during propane-CO_2 ODH reaction, thus eliminating this possibility for the observed catalyst deactivation (Table 1). In the fresh $12VO_x$/AC sample, the bands at 996, 700, 529, 478, 410, 287 and 142 cm^{-1} are visible, which is consistent with the presence of V_2O_3 [31]. This is in line with the XRD results (Fig. 5a). In the spent $12VO_x$/AC sample, four additional bands at 927, 877, 840 and 161 cm^{-1} are seen, which are characteristic for multi-valent vanadium states as present in V_6O_{13} [32, 33]. The formation of newly formed V_6O_{13} phase is likely related to exposure of finely dispersed V_2O_3 to highly reducing conditions during the propane-CO_2 ODH reaction.

In the $CeVO_4$/AC samples (Fig. 12b), only characteristic $CeVO_4$ Raman bands appear at 217, 257, 369, 463, 775 and 845 cm^{-1} [14]. In the fresh $30CeVO_4$/AC and $40CeVO_4$/AC samples, weak bands at 998 and 705 cm^{-1} are visible, which suggests presence of V_2O_3 in these samples. Their fraction is very likely minor, as they could not be identified through XRD.

4 Discussion

The initial propene selectivity of CeO_2/AC catalysts is low (16–27%) and stabilizes after 60 min of reaction at notably higher values (38–50%, Table 1). The re-oxidation of small

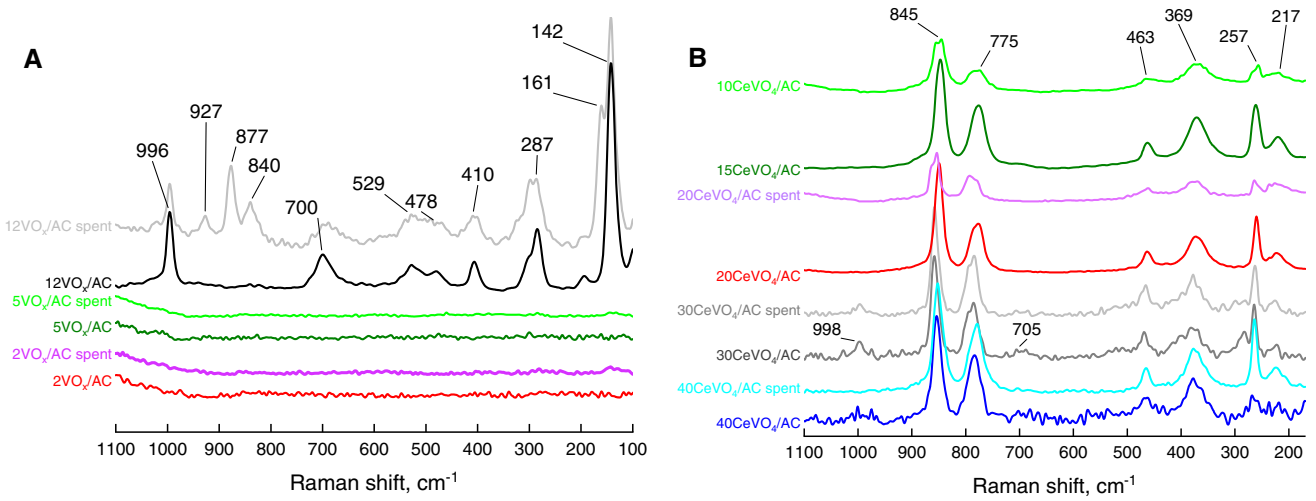

Fig. 12 **a** Stacked Raman spectra of fresh and spent VO_x/AC and **b** fresh and spent $CeVO_4$/AC catalysts. Please refer to online version of this manuscript for colour figure

CeO_{2-x} crystallites (4 nm), as present in CeO_2/AC catalysts with CO_2 occurs at higher temperatures compared to bulk CeO_2 (15 nm), revealing it is more difficult to dissociate CO_2 as the CeO_2 size decreases (Fig. 9a). This is consistent with structure sensitivity for CO_2 activation, namely the π-bond in C=O and TOF increases with increasing particle size, as a certain degree of site coordination is required [34, 35].

The propene selectivity appears to be influenced by the oxidation degree of CeO_{2-x}. Lower abundance of reactive surface oxygen sites in partly reduced CeO_{2-x} crystallites, when supported over AC compared to bulk CeO_2, provides less active sites for the activation of the C=C bond in propene. Consequently, higher propene selectivities are achieved over nanosized CeO_{2-x}.

Nowicka et al. [17] ascribed the initial deactivation of Pd/$CeAlO_x$ catalysts and a concomitant propene selectivity increase to the consumption of reactive oxygen species stored within the ceria lattice. These authors also suggest that the nonselective oxygen species, which are likely electrophilic, are singly charged interstitial oxygen anions. Once these O^- species are consumed, the catalyst can be re-oxidized by CO_2.

The fast deactivation and complete loss of propene selectivity over bulk V_2O_5 is related to its quantitative reduction from V^{5+} to V^{3+}, which leads to a progressive shift from propane ODH to propane cracking reaction. The CO_2-TPO experiment (Fig. 9c) revealed that bulk V_2O_3 cannot be re-oxidized by CO_2 at 550 °C. This shows the participation of CO_2 in the propane ODH reaction is negligible and the dominant ODH reaction pathway is governed by the availability of lattice oxygen in V_2O_5 and V_2O_4.

The reduction and re-oxidation dynamics of CeO_2 and V_2O_5 differ considerably, as could be observed by transient isothermal DRIFT spectroscopy analyses (Figs. 10 and 11). Propane interaction with CeO_2 leads to instantaneous and simultaneous CO_2 and CO formation which tail off slowly. Such behaviour is likely connected to the diffusion of lattice oxygen from the bulk to the surface [36], where it participates in the oxidation reactions.

Upon re-oxidation of CeO_{2-x} with CO_2, the polydentate carbonate signal stabilizes after 10 s of CO_2 addition, suggesting a kinetic preference for these species. The instantaneous appearance of a CO signal confirms facile CO_2 disproportionation and catalyst re-oxidation at 550 °C.

During V_2O_5 reduction with propane, the CO_2 signal lights off slowly and reaches a maximum at about 70 s after propane introduction. This suggests higher propane oxidation rates with lattice oxygen of CeO_2 compared to V_2O_5, which correlates also with notably higher initial propene selectivity over bulk catalysts (10% over CeO_2 and 27% over V_2O_5). CO appears after V=O overtone vibrations disappear (suggesting the absence of V^{5+} on the surface) [37].

At higher vanadium loadings in the VO_x/AC catalysts (12 wt%), a separate V_2O_3 phase is formed which is inert towards CO_2 and does not promote propane dehydrogenation. All VO_x/AC catalysts exhibit some deactivation with TOS, but propene selectivity remains constant (Table 1). Also, CO was identified as the reaction product during the entire duration of the catalytic tests and its concentration followed that of propene (Fig. S18), whereas the concentration of all other reaction products remained stable. This suggests that propene and CO are produced by the same oxidative dehydrogenation pathway (reaction 1). Considering that the fresh and spent catalysts contains no lattice oxygen (TEM-SAED, XRD and Raman analyses confirm a VC phase is formed exclusively at vanadium loadings up to

5 wt. %, whereas VC and V_2O_3 coexist at 12 wt. % vanadium loading), CO_2 remains as the only possible oxygen source. By combining the C_3H_8-TPR, CO_2-TPO and catalytic results we can postulate that CO_2 activation over the VC crystals is assisted by the adsorbed propane (protons at the methylene and methyl positions). In the absence of these electrophilic species which facilitate CO_2 decomposition [38] and H_2O formation, CO_2 activation requires temperatures close to 600 °C (Fig. 9c), which is above the reaction temperature used in this work. The deactivation of VO_x/AC catalysts is accompanied by a stable propene selectivity, which indicates that the total number of active sites, and not their nature, is changed with TOS. Oxidation of the VC phase during the propane-CO_2 ODH reaction does not occur, due to absence of V–O bonding in Raman spectra of the spent $2VO_x$/AC and $5VO_x$/AC catalysts. As a result, deactivation is probably related to blocking of active sites by carbon. Recently, Thakur et al. [39] report of in situ formation of oxycarbide phases (V_2O_3 and V_8C_7) during exposure of vanadium containing MXene catalysts to CH_4 and CO_2 atmosphere at much higher temperatures (800 °C).

The $CeVO_4$/AC catalysts showed the highest catalytic performance in terms of propene yields. Upon dispersion of $CeVO_4$ over activated carbon, a thin (1–2 nm) amorphous phase is formed over the $CeVO_4$ crystals. Its formation is likely connected to calcination in argon. The amorphous layer is intrinsically defective and the reactivity of oxygen in amorphous mixed metal oxides is higher than in any of its crystalline components [40]. Ruth et al. [41], report that the amorphous part of the multiphase Mo–V–Nb oxide catalyst is particularly important during oxidative dehydrogenation and partial oxidation of ethane.

During oxidative dehydrogenation of ethane, a transformation of VO_x/CeO_2 to $CeVO_4$ was identified by Martinez-Huerta et al. [14]. Based on the *operando* Raman analysis of the catalyst's structure, they identified the bridging oxygen atom (Ce–O–V) present in the ill-defined $CeVO_4$ phase as the active site for the rate determining step in the ODH reaction. Exposure to reaction temperatures above 500 °C favours crystallization of the $CeVO_4$ phase, making it inactive in the ODH reaction [14].

An increase of propane ODH catalytic activity scaled with the $CeVO_4$ loading. Catalytic activity is in line with the redox ability of the supported $CeVO_4$ phase, probed by propane and CO_2 (Figs. 8 and 9), which revealed lattice oxygen abstraction and re-oxidation are feasible under the reaction conditions. TEM analysis of the $CeVO_4$/AC catalyst after reaction revealed elimination of the amorphous $CeVO_4$ layer and the deposition of a few layers of carbon on the surface. This change is likely correlated to the observed catalyst deactivation. Since propene selectivity does not alter drastically with TOS (Figs. 2 and 3) despite notable deactivation, the number and not the nature of the active sites is decreased. A recent review of propane ODH with CO_2 by Atanga et al. [5] suggests that indium and especially gallium based catalysts are superior in activity and selectivity compared to chromium, platinum and vanadium based ones. When benchmarking the performance of best performing sample in this work ($30CeVO_4$/AC, 15.3% C_3H_8 conversion, 42% C_3H_6 selectivity, 6.4% C_3H_6 yield, C_3H_6 productivity of 9.5×10^{-5} mol/(g_{cat} min) at 550 °C, Table 2) with those reported over Ga_2O_3/Al_2O_3 by Michorczyk et al. [42], at 550 °C. A similar initial activity was observed (18% C_3H_8 conversion), but C_3H_6 selectivity was much higher (90%), corresponding to C_3H_6 productivity of 7.2×10^{-5} mol/(g_{cat} min). Xu et al. [43] tested several supports (TiO_2, SiO_2, ZrO_2 and MgO) for dispersing the active Ga_2O_3 phase. At 600 °C, the most active was Ga_2O_3/Al_2O_3, which enabled 26% conversion at 94% C_3H_6 selectivity, resulting in C_3H_6 productivity of 11.2×10^{-5} mol/(g_{cat} min).

Chen et al. [44] investigated how different supports (Al_2O_3, SiO_2 and ZrO_2) influence the propane ODH activity of 10 wt% In_2O_3 phase. At 600 °C, the highest propene selectivity of 85% was obtained In_2O_3/Al_2O_3 catalyst at a propane conversion of 20%, resulting in a propene productivity of 5.6×10^{-5} mol/(g_{cat} min).

Based on the above, the propene selectivity of best catalyst ($30CeVO_4$/AC) in this work is about twofold lower compared to those of Ga_2O_3 or In_2O_3 catalysts, but propene productivities are comparable.

5 Conclusions

The re-oxidation of small CeO_{2-x} crystallites (4 nm) with CO_2 occurs at higher temperatures compared to bulk CeO_2 (15 nm), revealing it is more difficult to dissociate CO_2 as the CeO_2 size decreases. Catalyst reduction by propane and re-oxidation by CO_2 are fast under reaction conditions and the propane dehydrogenation reaction proceeds via lattice oxygen participation. The Main reaction pathway over cerium containing catalysts is the total oxidation of propane.

Under propane-CO_2 ODH reaction conditions, V_2O_5 is irreversibly reduced to V_2O_3, which leads to a progressive shift from propane ODH to the propane cracking reaction. The participation of CO_2 in the ODH reaction is negligible and the reaction pathway is governed by the availability of lattice oxygen in V_2O_5 and V_2O_4. V_2O_3 preferentially catalyses propane cracking.

In the VO_x/AC catalysts, a VC phase is formed exclusively at vanadium loadings up to 5 wt%, whereas VC and V_2O_3 coexist at 12 wt% vanadium loading. By combining the C_3H_8-TPR, CO_2-TPO, and catalytic results we can postulate that CO_2 activation over the VC crystals is assisted by the adsorbed propane. As a result, the propane-CO_2 ODH reaction, over vanadium carbide, proceeds through

the Langmuir–Hinshelwood mechanism. The deactivation of VO_x/AC catalysts is accompanied with a stable propene selectivity, which indicates the total number of active sites and not their nature is changed with TOS. Oxidation of the VC phase during the propane-CO_2 ODH reaction does not occur due to the absence of any V–O bonding in spent catalysts. As a result, deactivation is probably related to blocking of the active sites by carbon.

The active site for the propane ODH reaction in the $CeVO_4$/AC catalysts is a thin (1–2 nm) amorphous $CeVO_4$ phase which covers the $CeVO_4$ crystals. Propane and CO_2-TPR experiments confirmed that during the propane ODH reaction lattice oxygen abstraction and re-oxidation are feasible, indicating active participation of CO_2 and a Mars van Krevelen reaction mechanism. During reaction, crystallization of the amorphous $CeVO_4$ layer and surface covering with carbon, which are the causes of catalyst deactivation.

Acknowledgements PD, IJ and JT acknowledge financial support through Research Programs P2-0150, P2-0393 and research Grant J7-7294 provided by the Slovenian Research Agency (ARRS). Mateja Knap, Katja Leskošek and Marko Vidic are kindly acknowledged for their assistance in catalyst synthesis and catalytic activity screening, Ervin Šest is acknowledged for performing the Raman analyses. The Cabot Company is kindly acknowledged for providing the Norit RX3 Extra activated carbon sample.

Compliance with Ethical Standards

Conflict of interest The authors declare no conflict of interest.

References

1. Carrero CA, Schlögl R, Wachs IE, Schomäcker R (2014) Critical literature review of the kinetics for the oxidative dehydrogenation of propane over well-defined supported vanadium oxide catalysts. ACS Catal 4:3357–3380. https://doi.org/10.1021/cs5003417
2. Khodakov A, Olthof B, Bell AT, Iglesia E (1999) Structure and catalytic properties of supported vanadium oxides: support effects on oxidative dehydrogenation reactions. J Catal 181:205–216. https://doi.org/10.1006/jcat.1998.2295
3. Kondratenko EV, Brückner A (2010) On the nature and reactivity of active oxygen species formed from O_2 and N_2O on VO_x/MCM-41 used for oxidative dehydrogenation of propane. J Catal 274:111–116. https://doi.org/10.1016/j.jcat.2010.06.010
4. Rozanska X, Fortrie R, Sauer J (2014) Size-dependent catalytic activity of supported vanadium oxide species: oxidative dehydrogenation of propane. J Am Chem Soc 136:7751–7761. https://doi.org/10.1021/ja503130z
5. Atanga MA, Rezaei F, Jawad A et al (2018) Oxidative dehydrogenation of propane to propylene with carbon dioxide. Appl Catal B 220:429–445. https://doi.org/10.1016/j.apcatb.2017.08.052
6. Wang S, Zhu ZH (2004) Catalytic conversion of alkanes to olefins by carbon dioxide oxidative dehydrogenation: a review. Energy Fuels 18:1126–1139. https://doi.org/10.1021/ef0340716
7. Baek J, Yun HJ, Yun D et al (2012) Preparation of highly dispersed chromium oxide catalysts supported on mesoporous silica for the oxidative dehydrogenation of propane using CO2: insight into the nature of catalytically active chromium sites. ACS Catal 2:1893–1903. https://doi.org/10.1021/cs300198u
8. Carrero C, Kauer M, Dinse A et al (2014) High performance $(VO_x)_n$–(TiO_x)m/SBA-15 catalysts for the oxidative dehydrogenation of propane. Catal Sci Technol 4:786. https://doi.org/10.1039/c3cy00625e
9. Cavani F, Ballarini N, Cericola A (2007) Oxidative dehydrogenation of ethane and propane: how far from commercial implementation? Catal Today 127:113–131. https://doi.org/10.1016/j.cattod.2007.05.009
10. Carley AF, Davies PR, Roberts MW (2011) Oxygen transient states in catalytic oxidation at metal surfaces. Catal Today 169:118–124. https://doi.org/10.1016/j.cattod.2010.10.081
11. Rozanska X, Kondratenko E, Sauer J (2008) Oxidative dehydrogenation of propane: differences between N_2O and O_2 in the reoxidation of reduced vanadia sites and consequences for selectivity. J Catal 256:84–94. https://doi.org/10.1016/j.jcat.2008.03.002
12. Michorczyk P, Ogonowski J (2003) Dehydrogenation of propane in the presence of carbon dioxide over oxide-based catalysts. React Kinet Catal Lett 78:41–47. https://doi.org/10.1023/A:1022501613772
13. Zou H, Ge X, Li M-S, Shangguan R-C, Shen J-Y (2000) Dehydrogenation of propane over CrO_x/SiO_2 catalysts under CO_2 atmosphere. Chin J Inorg Chem 1:775–782
14. Martínez-Huerta MV, Deo G, Fierro JLG, Bañares MA (2008) Operando Raman-GC study on the structure−activity relationships in V^{5+}/CeO_2 catalyst for ethane oxidative dehydrogenation: the formation of $CeVO_4$. J Phys Chem C 112:11441–11447. https://doi.org/10.1021/jp802827t
15. Ascoop I, Galvita VV, Alexopoulos K et al (2016) The role of CO_2 in the dehydrogenation of propane over WO_x–VO_x/SiO_2. J Catal 335:1–10. https://doi.org/10.1016/j.jcat.2015.12.015
16. Turakulova AO, Kharlanov AN, Levanov AV et al (2017) Catalytic properties of the $VO_x/Ce_{0.46}Zr_{0.54}O_2$ oxide system in the oxidative dehydrogenation of propane. Russ J Phys Chem A 91:17–25. https://doi.org/10.1134/S0036024417010307
17. Nowicka E, Reece C, Althahban SM et al (2018) Elucidating the role of CO_2 in the soft oxidative dehydrogenation of propane over ceria-based catalysts. ACS Catal 8:3454–3468. https://doi.org/10.1021/acscatal.7b03805
18. Rodríguez-Reinoso F (1998) The role of carbon materials in heterogeneous catalysis. Carbon N Y 36:159–175. https://doi.org/10.1016/S0008-6223(97)00173-5
19. Serp P, Corrias M, Kalck P (2003) Carbon nanotubes and nanofibers in catalysis. Appl Catal A Gen 253:337–358. https://doi.org/10.1016/S0926-860X(03)00549-0
20. Zhang X, Gao B, Creamer AE et al (2017) Adsorption of VOCs onto engineered carbon materials: a review. J Hazard Mater 338:102–123. https://doi.org/10.1016/j.jhazmat.2017.05.013
21. Cao L, Dai P, Zhu L et al (2020) Graphitic carbon nitride catalyzes selective oxidative dehydrogenation of propane. Appl Catal B

Environ 262:118277. https://doi.org/10.1016/j.apcatb.2019.118277
22. Węgrzyniak A, Jarczewski S, Kuśtrowski P, Michorczyk P (2018) Influence of carbon precursor on porosity, surface composition and catalytic behaviour of CMK-3 in oxidative dehydrogenation of propane to propene. J Porous Mater 25:687–696. https://doi.org/10.1007/s10934-017-0482-2
23. Boehm HP (1994) Some aspects of the surface chemistry of carbon blacks and other carbons. Carbon N Y 32:759–769. https://doi.org/10.1016/0008-6223(94)90031-0
24. Trovarelli A, Llorca J (2017) Ceria catalysts at nanoscale: how do crystal shapes shape catalysis? ACS Catal 7:4716–4735. https://doi.org/10.1021/acscatal.7b01246
25. Chakoumakos BC, Abraham MM, Boatner LA (1994) Crystal structure refinements of zircon-type MVO_4 (M = Sc, Y, Ce, Pr, Nd, Tb, Ho, Er, Tm, Yb, Lu). J Solid State Chem 109:197–202. https://doi.org/10.1006/jssc.1994.1091
26. Gamarra D, Belver C, Fernández-García M, Martínez-Arias A (2007) Selective CO oxidation in excess H_2 over copper−ceria catalysts: identification of active entities/species. J Am Chem Soc 129:12064–12065. https://doi.org/10.1021/ja073926g
27. Vayssilov GN, Mihaylov M, St PP et al (2011) Reassignment of the vibrational spectra of carbonates, formates, and related surface species on ceria: a combined density functional and infrared spectroscopy investigation. J Phys Chem C 115:23435–23454. https://doi.org/10.1021/jp208050a
28. Idriss H, Diagne C, Hindermann JP et al (1995) Reactions of acetaldehyde on CeO_2 and CeO_2-supported catalysts. J Catal 155:219–237. https://doi.org/10.1006/jcat.1995.1205
29. Jung S, Grange P (2002) DRIFTS investigation of V=O behavior and its relations with the reactivity of ammonia oxidation and selective catalytic reduction of NO over V_2O_5 catalyst. Appl Catal B Environ 36:325–332. https://doi.org/10.1016/S0926-3373(01)00314-9
30. Urbonaite S, Hälldahl L, Svensson G (2008) Raman spectroscopy studies of carbide derived carbons. Carbon N Y 46:1942–1947. https://doi.org/10.1016/j.carbon.2008.08.004
31. Xu G, Wang X, Chen X, Jiao L (2015) Facile synthesis and phase transition of V_2O_3 nanobelts. RSC Adv 5:17782–17785. https://doi.org/10.1039/C4RA13707H
32. Souza Filho AG, Ferreira OP, Santos EJG et al (2004) Raman spectra in vanadate nanotubes revisited. Nano Lett 4:2099–2104. https://doi.org/10.1021/nl0488477
33. Zhang C, Yang Q, Koughia C et al (2016) Characterization of vanadium oxide thin films with different stoichiometry using Raman spectroscopy. Thin Solid Films 620:64–69. https://doi.org/10.1016/j.tsf.2016.07.082
34. Vogt C, Kranenborg J, Monai M, Weckhuysen BM (2020) Structure sensitivity in steam and dry methane reforming over nickel: activity and carbon formation. ACS Catal 10:1428–1438. https://doi.org/10.1021/acscatal.9b04193
35. Vogt C, Groeneveld E, Kamsma G et al (2018) Unravelling structure sensitivity in CO_2 hydrogenation over nickel. Nat Catal 1:127–134
36. Vasiliades MA, Djinović P, Pintar A et al (2017) The effect of CeO_2-ZrO_2 structural differences on the origin and reactivity of carbon formed during methane dry reforming over NiCo/CeO_2-ZrO_2 catalysts studied by transient techniques. Catal Sci Technol. https://doi.org/10.1039/c7cy01009e
37. Wang J, Yan Z, Liu L et al (2014) In situ DRIFTS investigation on the SCR of NO with NH_3 over V_2O_5 catalyst supported by activated semi-coke. Appl Surf Sci 313:660–669. https://doi.org/10.1016/j.apsusc.2014.06.043
38. Vesselli E, Rizzi M, De Rogatis L et al (2010) Hydrogen-assisted transformation of CO_2 on nickel: the role of formate and carbon monoxide. J Phys Chem Lett 1:402–406. https://doi.org/10.1021/jz900221c
39. Thakur R, VahidMohammadi A, Smith J et al (2020) Insights into the genesis of a selective and coke-resistant MXene-based catalyst for the dry reforming of methane. ACS Catal 10:5124–5134. https://doi.org/10.1021/acscatal.0c00797
40. Schlögl R (2009) Concepts in selective oxidation of small alkane molecules. Modern heterogeneous oxidation catalysis. Wiley-VCH Verlag GmbH & Co. KGaA, Weinheim, pp 1–42
41. Ruth K, Burch R, Kieffer R (1998) Mo–V–Nb oxide catalysts for the partial oxidation of ethane. J Catal 175:27–39. https://doi.org/10.1006/jcat.1998.1976
42. Michorczyk P, Kuśtrowski P, Kolak A, Zimowska M (2013) Ordered mesoporous Ga_2O_3 and Ga_2O_3–Al_2O_3 prepared by nanocasting as effective catalysts for propane dehydrogenation in the presence of CO_2. Catal Commun 35:95–100. https://doi.org/10.1016/j.catcom.2013.01.019
43. Xu B, Zheng B, Hua W et al (2006) Support effect in dehydrogenation of propane in the presence of CO_2 over supported gallium oxide catalysts. J Catal 239:470–477. https://doi.org/10.1016/j.jcat.2006.02.017
44. Chen M, Wu J-L, Liu Y-M et al (2011) Study in support effect of In_2O_3/MO_x (M=Al, Si, Zr) catalysts for dehydrogenation of propane in the presence of CO_2. Appl Catal A Gen 407:20–28. https://doi.org/10.1016/j.apcata.2011.08.018